Journal of
Synchrotron
Radiation

ISSN 0909-0495

Received 6 November 2012
Accepted 23 January 2013

A reaction cell with sample laser heating for *in situ* soft X-ray absorption spectroscopy studies under environmental conditions

Carlos Escudero,[a] Peng Jiang,[b] Elzbieta Pach,[a] Ferenc Borondics,[b] Mark W. West,[c] Anders Tuxen,[a] Mahati Chintapalli,[a,d] Sophie Carenco,[a] Jinghua Guo[e] and Miquel Salmeron[a,d]*

[a]Materials Sciences Division, Lawrence Berkeley National Laboratory, 1 Cyclotron Road, Berkeley, CA 94720, USA, [b]Chemical Sciences Division, Lawrence Berkeley National Laboratory, 1 Cyclotron Road, Berkeley, CA 94720, USA, [c]Engineering Division, Lawrence Berkeley National Laboratory, 1 Cyclotron Road, Berkeley, CA 94720, USA, [d]Materials Science and Engineering Department, University of California, Berkeley, 210 Hearst Mining Building, Berkeley, CA 94720, USA, and [e]Advanced Light Source, Lawrence Berkeley National Laboratory, 1 Cyclotron Road, Berkeley, CA 94720, USA. E-mail: mbsalmeron@lbl.gov

A miniature (1 ml volume) reaction cell with transparent X-ray windows and laser heating of the sample has been designed to conduct X-ray absorption spectroscopy studies of materials in the presence of gases at atmospheric pressures. Heating by laser solves the problems associated with the presence of reactive gases interacting with hot filaments used in resistive heating methods. It also facilitates collection of a small total electron yield signal by eliminating interference with heating current leakage and ground loops. The excellent operation of the cell is demonstrated with examples of CO and H_2 Fischer–Tropsch reactions on Co nanoparticles.

© 2013 International Union of Crystallography
Printed in Singapore – all rights reserved

Keywords: *in situ*; laser heating system; soft X-ray absorption spectroscopy; heterogeneous catalysis; gas cell; nanoparticles.

1. Introduction

In recent years there has been a substantial effort to develop experimental techniques to perform microscopy and spectroscopy studies of surfaces under gas environments at realistic pressures with capabilities similar to those of well established surface science techniques that require high vacuum (Escudero & Salmeron, 2013). The reason for these efforts is the need to overcome the pressure gap between studies of well characterized surfaces in vacuum and those under realistic environments present in atmospheric science and industrial catalysis. It has indeed been demonstrated that the structure of the surface region of a material can be very different in *ex situ* vacuum experiments (*i.e.* exposed to gas reaction conditions and then measured under vacuum conditions) from that in dynamic equilibrium with the gas or liquid. For example, it has been shown (Tao *et al.*, 2008) that the surface composition of Pt–Rh nanoparticles (NPs) undergoes reversible changes under different gas compositions.

X-ray absorption spectroscopy (XAS) is an element-sensitive technique that can be applied to the study of the electronic structure of matter as it provides chemical information in the near-edge absorption region like oxidation state, as well as geometric information such as short-range geometry around the element under study, in the absorption oscillations farther from the edge (Stöhr, 1992). XAS requires a tunable source of photons, and it is widely used in synchrotron light facilities around the world. In the hard X-ray regime the high-energy photons travel deep into matter because of their low absorption coefficient. Soft XAS, on the other hand, can more easily access the *L*- and *M*-edges of lighter transition metals and other elements, information that is usually not available using the deep core *K*-edge spectra. In the soft X-ray energy regime the high absorption coefficient makes it necessary to work under low-pressure environments. In the last decade several gas and liquid cell designs have made it possible to study samples *in situ* under gas environments at atmospheric pressures (Knop-Gericke *et al.*, 1998; Hävecker *et al.*, 1999; Forsberg *et al.*, 2007; Zheng *et al.*, 2011) or under liquids (Fuchs *et al.*, 2008; Blum *et al.*, 2009; Tokushima *et al.*, 2009; Guo & Luo, 2010). Our group has been actively developing reactor cells for catalysis applications using gases (Herranz *et al.*, 2009), and for electrochemical applications under potentiostat control (Jiang *et al.*, 2010). In these cell designs the X-rays penetrate into the reaction volume through thin membranes, approximately 100 nm thick, made of Si_3N_4, Si or

Al. These membranes are strong enough to withstand the pressure difference between vacuum and the gas environment inside the cell, up to atmospheric pressures. XAS can be measured using fluorescence detection of the photons that exit the cell through the membrane, with the detector operating in the vacuum chamber. Although fluorescence detection is easy to implement and is the most widely used, it lacks surface sensitivity as the X-rays can travel several hundreds of nanometers in solid samples. Total electron yield (TEY), on the other hand, offers surface sensitivity because of the much shorter mean free path of low-energy electrons (less than a few 100 eV), which is of the order of nanometers. It also has the practical advantage of minimizing alignment problems with the detector.

In this paper we describe a new gas cell design that overcomes many shortcomings of previous designs, particularly problems associated with the heating of the sample under atmospheric gas pressures by using an IR laser heating system. The cell features lines for gas circulation and independent biasing of the cell cap for optimizing TEY detection.

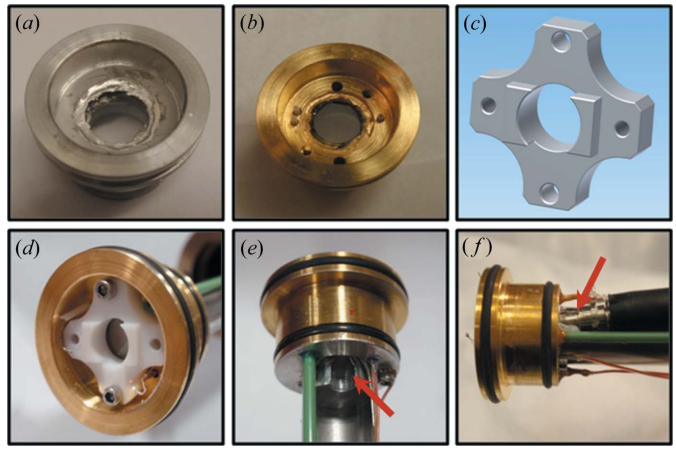

Figure 1
(*a*) Gas cell reactor with the quartz window covering the back; (*b*) as (*a*) but after gold sputtering; (*c*) ceramic sample support; (*d*) assembled sample support and cell chamber; (*e*) housing for the optical fiber mounted behind the quartz crystal (arrow); and (*f*) optical fiber attached at a 10° angle.

2. New gas cell with a novel laser heating system

2.1. Limitations of past designs

The cell design described in this paper overcomes many constraints from previous set-ups used for *in situ* XAS studies. One of the most important problems is related to sample heating in the presence of gases at atmospheric pressure. In previous systems resistive heating is commonly used. The filament is usually a Pt wire embedded in a ceramic. However, Pt is a well known catalyst in several reactions and during heating the filament is at a temperature higher than the sample itself, increasing the probability of its interaction with the reactant gases. This problem has been discussed recently (Chang *et al.*, 2012), showing that Pt resistive heaters in ambient-pressure X-ray photoelectron spectroscopy (Salmeron & Schlögl, 2008) can generate 'dark reactions' under catalytic reaction gas mixtures. The same applies to *in situ* XAS experiments if the heater is directly exposed to the gas reaction mixture. Even if the filament is embedded in a ceramic, its continuous use can create microfractures through which the gases can contact the filament. Heating to temperatures above 573 K often requires high currents and this can lead to leakage currents through the sample. Taking into account the small magnitude of the TEY current measured in XAS experiments, in the nano- or pico-ampere range, any leakage can substantially affect the measurements. A solution to these resistive heating problems is to use an infrared laser heating system (Günther *et al.*, 2006), which we will describe below.

Another important problem is the presence of materials that can interfere with the reactions studied. The reactor cell and gas supply system have to be made from materials that do not interact with the reactant gases, which could lead to the formation of compounds that can contaminate the surfaces, *e.g.* Fe and Ni carbonyls generated from stainless steel (Sykes *et al.*, 1993; Miksa & Brill, 2001). In our design these problems are avoided by coating all the materials in contact with the reactant gases with gold, and by using copper and brass for the gas lines and connections.

2.2. Reactor cell and laser heating system

The reactor cell consists of a gold-coated aluminium body (using a titanium adhesion layer of 15 nm; Fig. 1) with various feed-throughs for gas inlet and outlet, and for the wires used for thermocouples and for TEY current measurements. The TEY wire is shielded to minimize capacitive coupling, and the thermocouple wires are isolated from the reactor body by ceramic tubes sealed with high-temperature non-conductive epoxy (EPO-TEK H-70E; Epoxy Technology, Billerica, MA, USA). All the screws and clips used for fixing the sample are gold-coated. Fig. 2(*a*) shows the mounting of the reactor on the support tube that separates the cell from the UHV environment. A Si_3N_4 membrane (1.0 mm × 0.5 mm size and 100 nm thickness in square silicon supporting frames of 5 mm × 5 mm size and 200 µm thickness; Silson, Northampton, UK), semi-transparent to the X-rays, is glued to a gold-coated aluminium cap (Fig. 2*b*) using non-conductive epoxy. The cap slides over the tube on two elastomer O-rings (Viton Fluoroelastomer; McMaster-Carr, Chicago, IL, USA), which seal the reaction region while providing electrical isolation between the cap and the grounded reactor body. An independent line is used to pump the volume between the two O-rings. An additional cover cap (Fig. 2*c*) is screwed onto the tube over the cap with the membrane, with the two caps in electrical contact. The cover cap provides mechanical support as well as electrical bias for the cell. Biasing the cap helps prevent the Si_3N_4 window or sample from charging by photoemitted electrons or by gas ionized by the X-ray beam.

An infrared laser diode (class 4 laser with 18 A maximum current, maximum continuous output power of 10 W and

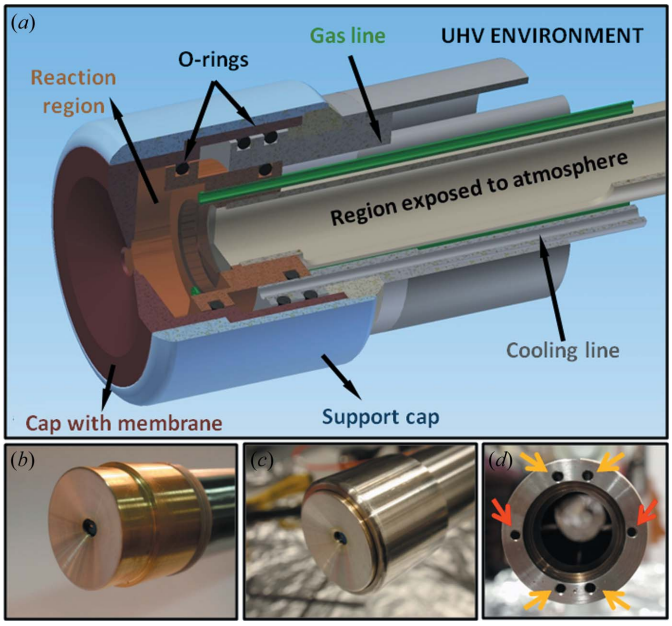

Figure 2
(*a*) Schematic of the gas cell showing one of the two gas lines (inlet/outlet) and one of the two inlet cooling lines. A quartz window (not shown) separates the reaction region from the support tube, which is exposed to atmospheric pressure. (*b*) Metallic cap with the Si_3N_4 membrane at the center. (*c*) Cover cap electrically connected to the one in (*b*). A bias can be applied to it to minimize signal interference from ionization of the reactant gases. (*d*) Front-view picture of the cell showing the two inlet orifices for the cooling lines (red arrows) and the four outlet holes connecting to the inside of the main tube (yellow arrows). This serves also to purge the main tube of any residual gas, such as oxygen.

975 nm wavelength; Axcel Photonics, Marlborough, MA, USA) is used to heat the sample, which sits on a ceramic support (Fig. 1*c*). The laser light illuminates the back of the sample through a fused quartz polished disc (10 mm × 2 mm; GM Associates, Oakland, CA, USA) sealing the back of the reactor. The quartz crystal has a high transmittance ($\geq$90%) at the laser wavelength and is connected to the reactor body (Fig. 1*a*) using a Sn–Ag–Ti-based low-temperature solder (S-Bond 220 Alloy; S-Bond Technologies LLC, Lansdale, PA, USA). The laser diode is located outside the gas cell and the light is conducted to the back of the sample through a fiber optic inside a stainless steel tube that is open to air and glued to the back of the reactor body. A small orifice at the end of this tube (Fig. 1*e*) holds the end of the optical fiber at ~5 mm distance from the center of the sample and at an angle of ~10° (Fig. 1*f*) to prevent reflections back into the fiber. Ideally the sample substrate should be chosen to absorb most of the laser light with low reflectivity to minimize heating of the reactor body. In our tests we found that the temperature distribution could be made very homogeneous across the entire sample surface using Au foils supported on Si wafers. A cooling system consisting of two inlet tubes and four outlet holes in the main tube to circulate N_2 gas is also built into the system to minimize temperature increases in the rest of the cell when heating for long periods of time [Figs. 2(*a*) and 2(*d*)]. In addition to its cooling function, the circulating gas purges the system from potential gas leaks in the cell. With this system the sample can reach temperatures above 773 K while the reactor temperature stays at <373 K, as shown in Fig. 3.

An important feature of our cell is the possibility of sample rotation and displacement forward and backward, which allows for exposure of new fresh areas to the X-ray beam. Increasing or decreasing the distance from the sample to the Si_3N_4 membrane is also important when the sample requires treatment to high temperature to minimize heating of the delicate Si_3N_4 membrane.

As safety is a key priority in our design, two main issues were considered. One is the possibility of undesired chemical reactions; for example leakages of reactant gases like H_2 can cause problems when mixed with air. As explained before, the cooling system provides an effective mitigation for potential interactions of H_2 and air because the cooling N_2 gas purges the line continuously. Another issue is the high power of the laser radiation. To prevent uncontrolled temperature increases from the laser and damage to the operator, an interlock system prevents the laser from being powered if the gas cell is not connected to the UHV chamber.

A schematic of the complete set-up, including the gas cell, gases and flow controllers, is shown in Fig. 4. In reactions utilizing CO, as in the Fischer–Tropsch example below, the gas cylinder is made of aluminium to avoid the formation of Ni and Fe carbonyls. A failure of the regulator or cylinder main valve would be moderated by a 0.15 mm restricted flow orifice on the cylinder output. In addition, a heated trap (523 K) filled with 10–40 mesh grain-size copper beads is used to remove traces of these unwanted contaminants. Although the system is designed to work at atmospheric pressure, a roughing pump is added to evacuate the gases after reaction as well as to operate the system at lower pressures (from a few Pa to

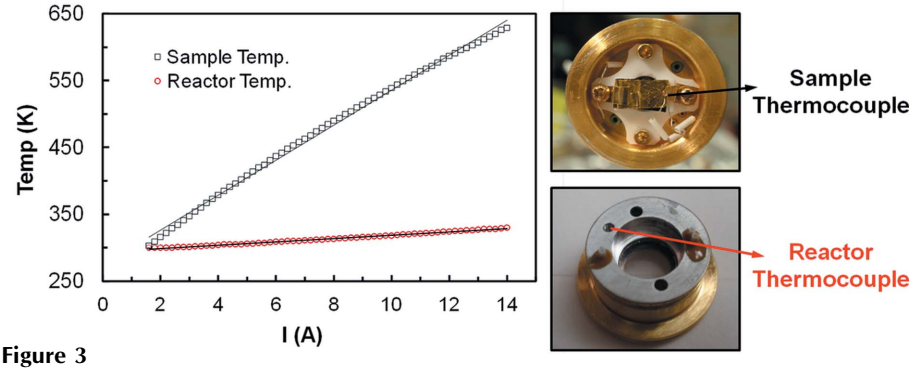

Figure 3
Graph of the sample temperature (black squares) and reactor wall temperature (red circles) as a function of laser pumping current (maximum current is 18 A). The pictures show the attachment point for the thermocouples. The experiments were performed using a gold foil sample (25 µm thick) supported on a doped Si substrate (350 µm thick) to improve absorption of the laser light and for temperature homogenization. During the experiments H_2 was flowed through the reactor cell at a 40 ml min^{-1} flow rate and 100 kPa. Cooling of the system is achieved by N_2 flow.

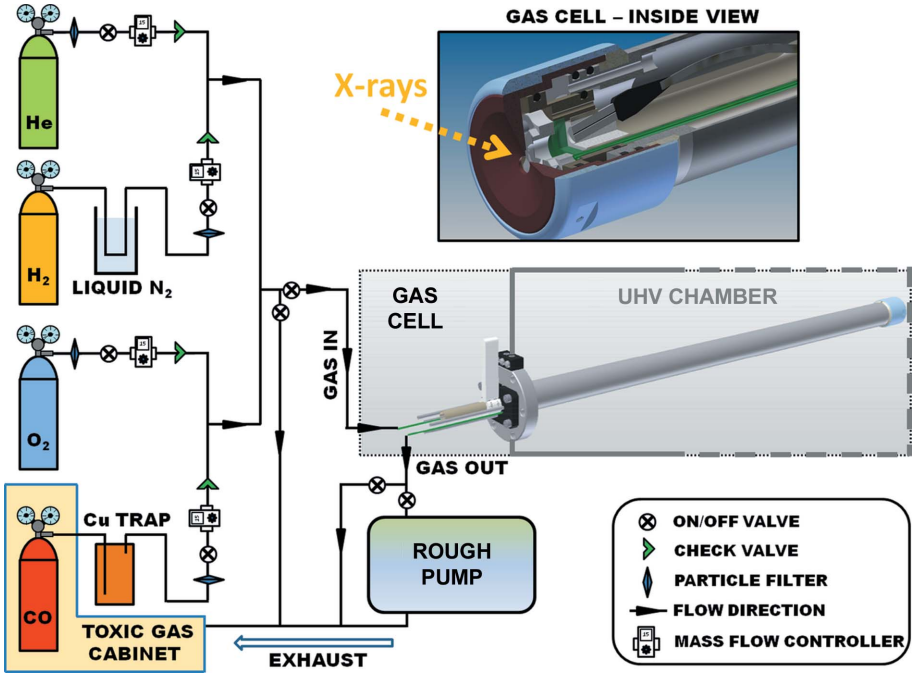

Figure 4
Schematics of the system set-up and inside view of the cell showing the position of the optical fiber behind the sample.

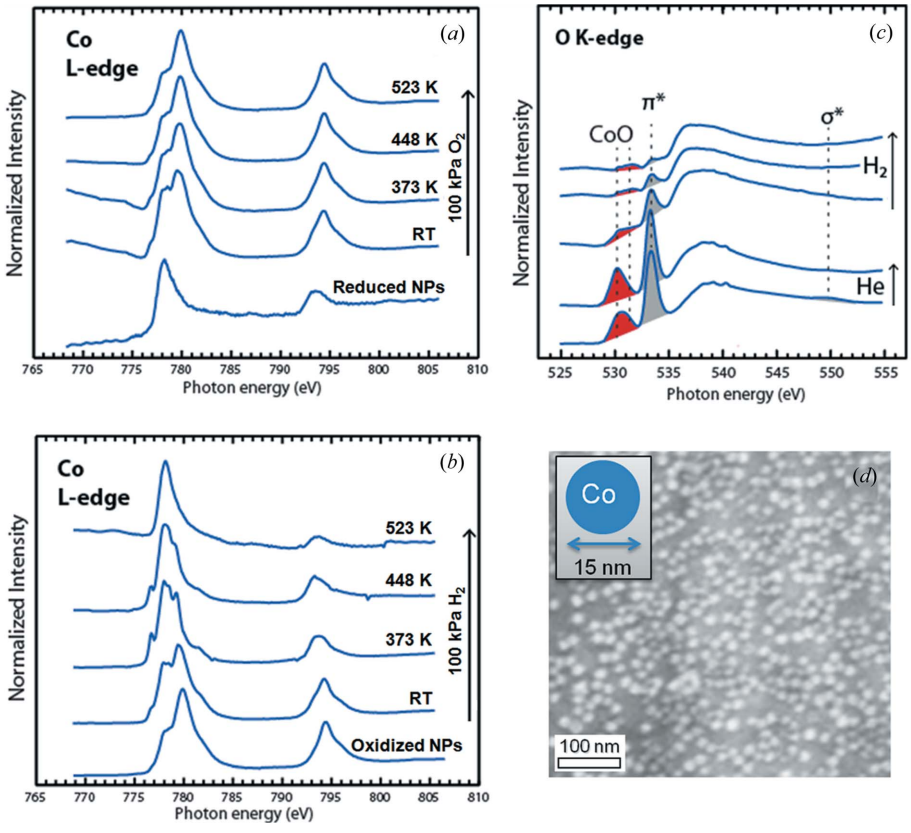

Figure 5
(*a*) Reference XAS spectra at the Co *L*-edge of reduced Co NPs (bottom spectrum) and oxidation states after heating under 100 kPa of O_2 at different temperatures. (*b*) Reduction of the oxidized NPs (bottom spectrum) under 100 kPa of H_2 at different temperatures. (*c*) XAS spectrum of the O *K*-edge region after first exposing the reduced nanoparticles to a mixture of CO and He and then to pure He or H_2. (*d*) Scanning electron microscope image of the 15 nm cobalt NPs as prepared.

atmospheric pressure) if desired. All gas lines are equipped with 2 µm pore size filters and calibrated mass flow controllers (Parker Hannifin Corporation, Porter Instrument Division, Hatfield, PA, USA) which maintain 5–50 ml min^{-1} flow rates.

3. Experimental case

To demonstrate the performance of the new cell design we show in Fig. 5 several XAS spectra of Co NPs, with 15 nm diameter (Fig. 5*d*), during oxidation and reduction in 100 kPa of H_2 and 100 kPa of O_2, respectively. These experiments were performed at beamline 7.0.1 of the Advanced Light Source, the Berkeley synchrotron, with an energy resolution of 0.3 eV. The Co NP samples were cleaned of surfactants and carbon-containing impurities by heating in 100 kPa of O_2 first, followed by reduction in 100 kPa of H_2 for several cycles. The reduced nanoparticles are characterized by a single asymmetric adsorption peak at 778 eV (Fig. 5*a*). During oxidation the peak evolves first to one characteristic of CoO and further to Co_3O_4 species. During reduction in 100 kPa of pure H_2 (Fig. 5*b*), the reverse sequence is obtained, reducing from Co_3O_4 to CoO at 373 K and finally to metallic cobalt at 523 K. This study, and the subsequent Fischer–Tropsch reaction studies under CO and H_2 atmospheres, could not have been observed without the *in situ* techniques described here since Co is very reactive and is easily oxidized and contaminated by exposure to air, or even in vacuum. The H_2 atmosphere dynamically maintains the Co clean and in the metallic state. Fig. 5(*c*) shows an XAS spectrum in the region of the O *K*-edge after exposing the reduced nanoparticles to CO. The lower spectrum displays adsorption features typical of the diatomic molecule, *i.e.* a strong π^* adsorption feature at 534 eV and a weak σ^* at 550 eV. Upon exposure to H_2, the π^* peak decreases with time due to reactions that produce methane. An extensive account of the initial reaction steps has been published recently (Tuxen *et al.*, 2013).

4. Conclusions

In summary, we have described a new and improved gas cell designed to perform soft XAS experiments under reaction conditions. This design overcomes many limitations of previous designs. An important novelty is a laser heating system that eliminates problems associated with resistive heating, namely unwanted reactions on the resistor's catalytically active surface, and current leakages through the sample that make TEY XAS measurements difficult or impossible. The samples can be heated to temperatures higher than 773 K, while the reactor cell body temperature stays below 373 K. The cell can operate in batch or flow mode from a few Pa to atmospheric pressure of any gas.

This work was supported by the Director, Office of Energy Research, Division of Materials Sciences and Engineering of the US Department of Energy under Contract No. DE-AC02-05CH11231. CE acknowledges financial support from the MEC/Fulbright program (reference No. 2008-0253). AT acknowledges the support from the Danish Research Council for Independent Research Natural Sciences (Det Frie Forskningsraad Natur og Univers).

References

Blum, M., Weinhardt, L., Fuchs, O., Bär, M., Zhang, Y., Weigand, M., Krause, S., Pookpanratana, S., Hofmann, T., Yang, W., Denlinger, J. D., Umbach, E. & Heske, C. (2009). *Rev. Sci. Instrum.* **80**, 123102.

Chang, R., Hong, Y. P., Axnanda, S., Mao, B., Jabeen, N., Wang, S., Tai, R. & Liu, Z. (2012). *Curr. Appl. Phys.* **12**, 1292–1296.

Escudero, C. & Salmeron, M. (2013). *Surf. Sci.* **607**, 2–9.

Forsberg, J., Duda, L. C., Olsson, A., Schmitt, T., Andersson, J., Nordgren, J., Hedberg, J., Leygraf, C., Aastrup, T., Wallinder, D. & Guo, J. H. (2007). *Rev. Sci. Instrum.* **78**, 083110.

Fuchs, O., Maier, F., Weinhardt, L., Weigand, M., Blum, M., Zharnikov, M., Denlinger, J., Grunze, M., Heske, C. & Umbach, E. (2008). *Nucl. Instrum. Methods Phys. Res. A*, **585**, 172–177.

Günther, S., Zhou, L., Hävecker, M., Knop-Gericke, A., Kleimenov, E., Schlögl, R. & Imbihl, R. (2006). *J. Chem. Phys.* **125**, 114709.

Guo, J. & Luo, Y. (2010). *J. Electron Spectrosc. Relat. Phenom.* **177**, 181–191.

Hävecker, M., Knop-Gericke, A. & Schedel-Niedrig, T. (1999). *Appl. Surf. Sci.* **142**, 438–442.

Herranz, T., Deng, X., Cabot, A., Guo, J. & Salmeron, M. (2009). *J. Phys. Chem. B*, **113**, 10721–10727.

Jiang, P., Chen, J., Borondics, F., Glans, P., West, M. W., Chang, C., Salmeron, M. & Guo, J. (2010). *Electrochem. Commun.* **12**, 820–822.

Knop-Gericke, A., Hävecker, M., Neisius, T. & Schedel-Niedrig, T. (1998). *Nucl. Instrum. Methods Phys. Res. A*, **406**, 311–322.

Miksa, D. & Brill, T. B. (2001). *Ind. Eng. Chem. Res.* **40**, 3098–3103.

Salmeron, M. & Schlögl, R. (2008). *Surf. Sci. Rep.* **63**, 169–199.

Stöhr, J. (1992). *NEXAFS Spectroscopy*. Berlin: Springer-Verlag.

Sykes, M., Edwards, I. & Thomas, K. (1993). *Carbon*, **31**, 467–472.

Tao, F., Grass, M. E., Zhang, Y., Butcher, D. R., Renzas, J. R., Liu, Z., Chung, J. Y., Mun, B. S., Salmeron, M. & Somorjai, G. A. (2008). *Science*, **322**, 932–934.

Tokushima, T., Horikawa, Y., Harada, Y., Takahashi, O., Hiraya, A. & Shin, S. (2009). *Phys. Chem. Chem. Phys.* **11**, 1679–1682.

Tuxen, A., Carenco, S., Chintapalli, M., Chuang, C.-H., Escudero, C., Pach, E., Jiang, P., Borondics, F., Beberwyck, B. J., Alivisatos, A. P., Thornton, G., Pong, W.-F., Guo, J., Perez, R., Besenbacher, F. & Salmeron, M. (2013). *J. Am. Chem. Soc.* **135**, 2273–2278.

Zheng, F., Alayoglu, S., Guo, J., Pushkarev, V., Li, Y., Glans, P. A., Chen, J. L. & Somorjai, G. (2011). *Nano Lett.* **11**, 847–853.